Surface energy fluxes with the Advanced Spaceborne Thermal Emission and Reflection radiometer (ASTER) at the Iowa 2002 SMACEX site (USA)

Andrew Nichols French, Frederic Jacob, Martha Anderson, W.P. Kustas, W. Timmermans, A. Gieske, Z. Su, H. Su, M.F. Mccabe, F. Li, et al.

Editorial Manager(tm) for Remote Sensing of Environment
Manuscript Draft

Manuscript Number: RSE-D-04-00907R3

Title: Surface energy fluxes with the Advanced Spaceborne Thermal Emission and Reflection radiometer (ASTER) at the Iowa 2002 SMACEX site (USA)

Article Type: Special Issue Papers

Section/Category:

Keywords: Thermal infrared; ASTER; high spatial resolution; multispectral TIR; surface energy balance modeling; spatial variability

Corresponding Author: Dr. Andrew N. French,

Corresponding Author's Institution: USDA/ Agricultural Research Service

First Author: A. N. French

Order of Authors: A. N. French; F Jacob, PhD; M C Anderson, PhD; W P Kustas, PhD; W Timmermans; A Gieske; Z. Su; H Su; M F McCabe; F Li; J Prueger; N Brunsell

Manuscript Region of Origin:

Surface Energy Fluxes with the Advanced Spaceborne Thermal Emission and Reflection Radiometer (ASTER) at the Iowa 2002 SMACEX site (USA).

A. N. French *

U.S. Water Conservation Lab, USDA/ARS, 4331 E. Broadway Rd., Phoenix, AZ 85040 USA

F. Jacob

Remote Sensing and Territory Management Laboratory, PURPAN- Graduate School of Agriculture, 75 Voie du TOEC, 31076 Toulouse Cedex 3 France

M.C. Anderson

Department of Soil Science, University of Wisconsin-Madison, 1525 Observatory Drive, Madison, WI 53706 USA

W.P. Kustas

Hydrology & Remote Sensing Lab, USDA/ARS, Bldg 007, BARC West, Beltsville, MD USA

W. Timmermans

Preprint submitted to Remote Sensing of Environment *6 May 2005*

International Institute for Geo-Information Science and Earth Observation (ITC), Hengelosestraat 99, P.O. Box 6, 7500 AA Enschede, The Netherlands

A. Gieske

International Institute for Geo-Information Science and Earth Observation (ITC), Hengelosestraat 99, P.O. Box 6, 7500 AA Enschede, The Netherlands

B. Su

International Institute for Geo-Information Science and Earth Observation (ITC), Hengelosestraat 99, P.O. Box 6, 7500 AA Enschede, The Netherlands

H. Su

Dept of Civil & Environmental Engineering, Princeton University, Princeton, NJ 08544 USA

M. F. McCabe

Dept of Civil & Environmental Engineering, Princeton University, Princeton, NJ 08544 USA

F. Li

Hydrology & Remote Sensing Lab, USDA/ARS, Bldg 007, BARC West, Beltsville, MD USA

J. Prueger

National Soil Tilth Research Lab, Ames, Iowa 50011 USA

N. Brunsell

Dept of Geography, University of Kansas, Lindley Hall 117, 1475 Jayhawk Blvd.

Lawrence, KS

Abstract

Accurate estimation of surface energy fluxes from space at high spatial resolution has the potential to improve prediction of the impact of land-use changes on the local environment and to provide a means to assess local crop conditions. To achieve this goal, a combination of physically based surface flux models and high-quality remote-sensing data are needed. Data from the ASTER sensor are particularly well-suited to the task, as it collects high spatial resolution (15 - 90 m) images in visible, near-infrared, and thermal infrared bands. Data in these bands yield surface temperature, vegetation cover density, and land-use types, all critical inputs to surface energy balance models for assessing local environmental conditions. ASTER is currently the only satellite sensor collecting multispectral thermal-infrared images, a capability allowing unprecedented surface temperature estimation accuracy for a variety of surface cover types. Availability of ASTER data to study surface energy fluxes allows direct comparisons against ground measurements and facilitates detection of modeling limitations, both possible because of ASTER's higher spatial resolution.

Surface energy flux retrieval from ASTER is demonstrated using data collected over an experimental site in central Iowa, USA, in the framework of the Soil Moisture Atmosphere Coupling Experiment (SMACEX). This experiment took place during the summer of 2002 in a study of heterogeneous agricultural croplands. Two different flux estimation approaches, designed to account for the spatial variability, are considered: the Two-Source Energy Balance model (TSEB) and the Surface Energy Balance Algorithm for Land model (SEBAL). ASTER data are shown to have spatial and spectral resolution sufficient to derive surface variables required as inputs for physically based energy balance modeling. Comparison of flux model

results against each other and against ground based measurements was promising, with flux values commonly agreeing within ∼50 W m^{-2}. Both TSEB and SEBAL showed systematic agreement and responded to spatially varying surface temperatures and vegetation densities. Direct comparison against ground Eddy Covariance data suggests that the TSEB approach is helpful over sparsely vegetated terrain.

Key words:

Thermal infrared, ASTER, high spatial resolution, multispectral TIR, surface energy balance modeling, spatial variability

1 Introduction

The Advanced Spaceborne Thermal Emission and Reflection Radiometer (ASTER) is a special remote-sensing tool intended to help estimate the surface energy balance, a critical attribute for monitoring land surface climate, hydrological processes and vegetation health. Using ASTER observations with spatial resolutions ranging from 15 to 90 m, in combination with a model simulating energy transfer, detailed estimates of surface energy fluxes may potentially be retrieved over large portions of the Earth's landmass. Knowledge of energy fluxes is important, providing meteorological boundary conditions for convection within the atmospheric boundary layer, and evapotranspiration (ET) estimates for hydrological studies, including vegetation transpiration estimates for crop growth assessment. The required flux retrieval accuracy varies by application, but is typically ∼50 W m^{-2}, as suggested by Seguin et al. (1999).

* Corresponding author. Address:
Email address: afrench@uswcl.ars.ag.gov (A. N. French).

The essential idea for energy flux estimation of ET is recognition that water vapor mass transport can equivalently be represented as energy transport. Due to the large amount of heat represented by the evaporation process, water mass transport can be accurately estimated from known energy transport. Since energy transport of water vapor is directly connected to thermal and water vapor gradients, one can estimate ET primarily from knowledge of four quantities: surface temperature, vegetation density, near surface air temperature and near surface humidity. The first two are readily estimated from remote-sensing, while the last two are obtainable from ground observations or possibly from remote-sensing contextual data.

Estimation of land surface ET is of course not new, and in recent years accurate point-based observations have been used to monitor ET variability at hourly time scales. Examples include experiments at Monsoon '90 (Stannard et al., 1994), FIFE (Kanemasu et al., 1992; Shuttleworth et al., 1989), HAPEX-SAHEL (Goutorbe et al., 1994), EFEDA (Pelgrum and Bastiaanssen, 1996), BOREAS (Sellers et al., 1997), NOPEX (Halldin and Gryning, 1999), JORNEX (Havstad et al., 2000) and ReSeDA (Olioso et al., 2002b). However, it has also been recognized that spatially variability of ET is large and that even the most advanced ways of measuring ET with tower-mounted Eddy Covariance (E-C) systems are often not representative of landscape scale ET (Stannard et al., 1994; Pelgrum and Bastiaanssen, 1996). Consequently, incorporation of remote-sensing data is required, since this is the only way to simultaneously observe surface properties over large surface areas.

ET monitoring with remote sensing has yet to be proven as a reliable, robust approach. Recent experiments show promising results, with systematic agreement between estimates from ground and aircraft measurements over several

test areas (French et al., 2003; Kustas et al., 1994; Moran et al., 1994; Norman et al., 1995; Kustas et al., 1996; Zhan et al., 1996; Anderson et al., 1997; Norman et al., 2000; Hasager et al., 2002; Wassenaar et al., 2002; Jacob et al., 2002a; Olioso et al., 2002a). On the other hand, previous criticisms (e.g., Hall et al., 1992) suggest that thermal infrared (TIR) satellite observations, particularly, are not sufficiently accurate to constrain flux models. Although such critiques have been refuted (Kustas and Norman, 1999; Bastiaanssen et al., 1998a,b), further examples are clearly needed before remote sensing can be used operationally for this purpose.

Accurate spatially distributed estimates of surface energy fluxes require physically based energy flux models driven by accurate remote-sensing observations. Such ideal models, which do not depend on empirical calibration, are unrealizable since complete consideration of processes at the local scale requires large amounts of unavailable information. Some models (e.g., SiB2, Sellers et al., 1986) estimate ET from the Penman-Monteith equation (Penman, 1948; Monteith and Unsworth, 1990), which considers both the radiative flux and the water mass flux, and can use remote sensing to derive net radiation (R_n). This widely used approach, however, does not adequately model heterogeneous surfaces or water-stressed vegetation. Other approaches, such as the simplified method of Jackson et al. (1977), can model some of these conditions by incorporating surface temperatures observed from thermal remote sensing, but do so in an empirical way, meaning that local calibration is required.

Recent versions of remote-sensing energy flux models have progressed to include treatment for a wide range of conditions including heterogeneous surfaces and variable meteorological constraints, thereby reducing problems encountered previously. These newer models are similar in some respects to pre-

decessors such as Penman-Monteith models, but represent an advance to the state of the art because they incorporate higher spectral and spatial resolution remote-sensing data across the visible, near-infrared and thermal wavelengths. Five examples are: the Two Source Energy Balance model (TSEB, Norman et al., 1995), DisAlexi (Norman et al., 2003), the Surface Energy Balance Algorithm for Land model (SEBAL, Bastiaanssen et al., 1998a), the Surface Energy Balance System (SEBS, Su, 2002), and the NDVI/Temperature triangle method (Gillies et al., 1997). Although these models rely upon different assumptions and interpret remote-sensing data in different ways, they have all been tested and verified under local conditions. This means that any one of them ought to return accurate surface flux estimates given accurate input observations. However the question remains whether or not these models are generally applicable and can do what previous models could not, namely reliably estimate spatially distributed surface energy fluxes.

One way to answer this question is to assemble multispectral remote-sensing observations of high quality and high spatial resolution over various landscapes and to compare model results with each other and with independently measured ground flux measurements. In this respect, ASTER should be well-suited to the task since it can accurately retrieve vegetation density, spectral reflectances over visible and near-infrared (VNIR) wavelengths (Jacob et al., 2002b), and surface temperatures potentially accurate to $\sim$0.5°C (Hook and Prata, 2001). In recent work by Jacob et al. (2004), land surface temperature retrieval agreement between ASTER and MODIS sensors was $\sim$0.9°C , indicating consistent data quality.

In this paper we demonstrate estimation of surface energy fluxes using ASTER data by examining first results from a model intercomparison study based on

observations over a 2002 experimental study in Iowa, USA. The approach is to first discuss basic observational requirements for landscape-scale surface energy balance modeling and how ASTER data meet those requirements. Next we briefly describe implementations of the TSEB and SEBAL models. Third, these flux models are compared with each other and ground-level measurements.

2 Observational Requirements

Regardless of spatial scale, estimation of surface energy fluxes (Brutsaert, 1982; McNaughton and Spriggs, 1989) can be represented by the balance of turbulent fluxes against available energy:

$$\mathrm{H} + \mathrm{LE} = \mathrm{R_n} - \mathrm{G} \tag{1}$$

where H, sensible heat and LE, latent heat, are turbulence terms, G is conducted soil heat and $\mathrm{R_n}$ is net radiation. These terms, all in W $\mathrm{m^{-2}}$, respectively represent energy conducted away from the surface and energy delivered to the Earth's surface. Neglected are storage and photosynthesis terms. These latter two terms are usually thought unimportant for short-term estimates over non-forested areas. However, recent work by Meyers and Hollinger (2004) suggests that storage in corn fields can be significant. Spatial implementation of Eq.1 requires an underlying energy balance model and boundary condition constraints from remote sensing data observations. Terms in Eq.1 constrained by remote sensing depend upon spatial and spectral resolutions. Using VNIR to TIR detectors, constraints on three of four terms are directly possible: H, $\mathrm{R_n}$ and G. H is constrained by surface temperatures derived from TIR data, while

both R_n and G fluxes are constrained by both VNIR reflectances and emitted TIR radiances. The remaining component, LE can be constrained indirectly by residuals.

The useful role of VNIR-TIR remote-sensing in energy flux modeling is therefore determined by a sensor's ability to accurately determine the three flux terms from observed reflected and emitted radiances. Without sufficient accuracy, errors from estimates of H, R_n and G accumulate in LE flux estimates and could overwhelm results by 100's of W m^{-2} (Kustas and Norman, 1996).

For this paper we examine ASTER's suitability by evaluating results from an experimental site in central Iowa known as the Soil Moisture Atmosphere Coupling Experiment 2002 (SMACEX). The site consisted of intensive soil, vegetation and meteorological observations over the Walnut Creek Watershed, an area just south of Ames, Iowa, USA (Kustas et al., 2004). Two observational factors we consider are spatial and spectral resolution.

2.1 Spatial Resolution

For surface energy balance modeling the chief requirement for spatial resolution is the ability to distinguish land cover types that have distinctly different heat flux properties and resolve spatial variability of the considered processes within a land-class type. Over agricultural regions, these cover types include grazinglands, managed crops, riparian zones, water bodies and fields of bare soil. Each of these types differs significantly in surface roughness, potential heat capacity, moisture content, and spectral reflectance. Spatial variability of energy fluxes at local scales is strongly controlled by soil and micro-

meteorological conditions.

ASTER images are potentially able to make these distinctions over all three band groups, with 15-m resolution for VNIR bands 1,2 and 3; 30-m resolution for SWIR bands 4-9; and 90-m resolution for TIR bands 10-14 (Yamaguchi et al., 1998). Considering the context of currently available images (e.g., Ikonos, Quickbird, TM7 and MODIS), ASTER data may be considered high- to moderate-resolution because they match TM7's capabilities in visible and near infrared wavelengths and have a significantly higher resolution than MODIS' best resolution (250 m).

An example of ASTER's spatial capability can be demonstrated using SMACEX imagery from 1 July 2002. Using 15-m NDVI images (Fig. 1), land-use patterns and highways are clearly defined at the landscape scale. NDVI was derived from Level 2 ASTER processing of band 2 and 3N reflectances (Abrams, 2000).

In the Iowa example above, the adequacy of remote-sensing resolution was determined qualitatively, where imagery was checked against expected land cover patterns at the section and quarter section levels. Knowing that adequate resolution must be about half the distance of the dominant land-surface scale to avoid dominance of mixed pixels (e.g., Woodcock and Strahler, 1987), minimal resolution over SMACEX is $\sim$1/8 mile (400 m). A more quantitative way to evaluate land-surface scales and required resolution, is to generate histograms at successively coarser resolutions and assess where the distributional pattern changes. Using ASTER 15-m NDVI images, landscape scale is identified from a series of histograms generated from image reflectance aggregations. In the SMACEX NDVI example (Fig. 3), source red and near-infrared

reflectance data were aggregated by spatial averaging to 90 m (ASTER TIR nominal resolution) and 240 m (close to 250 m, the best MODIS nominal resolution), then combined to yield NDVI. Since NDVI is closely coupled to energy balance model results, knowing the minimum resolution needed to represent relatively homogeneous areas of vegetation, rather than as clumped mixtures is important. Histograms shown in Fig. 3 indicate that the minimum required resolution is somewhere between 90-m and 240-m resolutions due to a significant distributional change. At 15- to 90-m spatial resolutions, vegetation cover is bimodally distributed. At 240-m resolution, the bimodal distribution is mostly lost, meaning that distinctive sparse vegetation values are mixed with dense vegetation ones.

A critical spatial issue for energy balance modeling is the ability to distinguish land-use patterns in the TIR. Surface temperature, rather than vegetation density, is the most influential parameter for instantaneous energy fluxes. ASTER surface temperature data collected over SMACEX with a 90-m spatial resolution resolves dominant land-use patterns discerned with VNIR data (Fig. 2). Surface temperatures, derived from the Temperature Emissivity Separation (TES) algorithm (Gillespie et al., 1998) and atmospherically corrected with radiosonde data and MODTRAN (Berk et al., 1998), range between 25 and 40°C for the 17:12UT (12:12CDT) overpass time. Lower temperatures correspond to thickly vegetated areas and warmer temperatures to sparsely vegetated areas. As shown, patchwork patterns, mainly representing corn and soybean fields, are readily discerned, as are riparian zones to the east and urban areas to the north. This means that physically representative energy flux modeling is feasible at this site at 90-m scales, and potentially at 15-m scales by applying a thermal sharpening technique described in Kustas et al. (2003).

In addition to requiring sufficient spatial resolution, successful estimation of surface energy fluxes requires sufficient spectral resolution to create vegetation density and land surface temperature image estimates. The first three ASTER bands (1,2 and 3) sample green to near-infrared wavelengths (0.52 to 0.86 μm) and are suitable for NDVI and albedo images compatible with TM data. Though some bandwidths are not as optimal as found elsewhere— MODIS band 2 (0.84-0.88 μm) is narrower than ASTER's band 3 (0.76-0.86 μm), and hence less sensitive to atmospheric water vapor content— the calibration levels are excellent, with signal to noise ratios greater than 56 at 15-m spatial resolution [Earth Remote Sensing Data Center (ERSDAC), 2001]. The next six bands (4-9) non-contiguously sample short-wave infrared (SWIR) over 1.6-2.43 μm. Though not used in this study, these SWIR bands can be used to improve land cover characterization and surface albedo estimates. Finally, five TIR bands (10-14) sample wavelengths in two groups: one for 8.125-9.275 μm, an interval frequently diagnostic of high emissivity contrast surfaces, and another for 10.25-11.65 μm, where emissivity variations are commonly small (Fig. 4).

ASTER's multispectral TIR imaging capability is its most distinguishing characteristic and is important for retrieving surface temperatures, potentially accurate to 0.5°C . Reasons for this potential are its low NEΔT (noise-equivalent change in temperature, a measure of the signal-to-noise ratio for thermal detectors), <0.3 K, and its multiband placement within the TIR window Five TIR bands allow better estimation of spectral variability of surface brightness temperatures and surface emissivities (Gillespie et al., 1998) than otherwise

achievable with single-band or split-window approaches.

3 Energy Flux Modeling

To show how ASTER can be used to model the surface energy fluxes, we combine ASTER imagery over the SMACEX site with implementations of two well-known energy balance models, the Two Source Energy Balance approach (TSEB, Norman et al., 1995), and the Surface Energy Balance Algorithm for Land approach (SEBAL Bastiaanssen et al., 1998a). By showing results from two models, rather than one, model performance can be seen for the same landscape, and allows identification of model strengths and weaknesses.

3.1 TSEB

TSEB is a remote-sensing two-source approach based upon land surface separability into two distinct, but linked components: soil surfaces and vegetation canopies. By combining remote observations of surface temperature, vegetation data, land cover class, and near-surface meteorological data, surface resistance characteristics can be modeled in a more physically meaningful way (Kustas and Norman, 2000, 1999) than a more typical one-source approach based on the kB^{-1} parameter (Garratt and Hicks, 1973). TSEB derives energy flux estimates from modeling the land as a resistance network, between energy sources from soil, vegetation, and the overlying atmosphere. Two main variants of TSEB exist, one applicable strictly at local scales (as described in Norman et al., 1995), while the other, known as DisAlexi (Anderson et al., 1997; Mecikalski et al., 1999) is also useful at regional scales since it also

models energy exchange at the atmospheric boundary layer. The model outputs used here are from the DisAlexi implementation of TSEB, but we note that results from the local implementation are similar due to the local scale of SMACEX. R_n, computed from a multiple scattering model (Monteith and Unsworth, 1990; Goudriaan, 1977) is partitioned for each of the considered spectral ranges: visible, near-infrared and TIR wavelengths (Norman et al., 1995). This partitioning allows discrimination between energy available at the soil surface and energy delivered to the vegetation canopy. TSEB has three key assumptions: turbulent fluxes are constant within the near surface layer (Monin-Obukhov similarity is used for stability correction), radiometric temperature can be repartitioned into soil and vegetation components, and Priestley-Taylor transpiration (Priestley and Taylor, 1972) applies for unstressed vegetation. More complete details are described in Norman et al. (1995) and in French et al. (2003).

3.2 SEBAL

The SEBAL model, in contrast to TSEB, is a one-source modeling approach which does not discriminate soil and vegetation components. This model is based upon the estimation of surface energy fluxes with minimal ancillary information by considering spatial variability within the images themselves. This design principal has great practical value since instantaneous evapotranspiration estimates can potentially be retrieved worldwide without the need to collect ground-based data. SEBAL does this by contextual separation of the land-surface images into 'wet' and 'dry' areas. Distinction is achieved using the 'evaporative controlled' and 'radiative controlled' branches of a surface

temperature-versus-albedo diagram. If both areas are included within the images, the diagram commonly shows a characteristic parabolic pattern. The vertex marks the maximum observed radiometric temperature and separates the lower albedo wet areas from the higher-albedo dry areas.

An aggregation scheme of the dry area properties is used along with air temperature at an estimated blending height in order to compute a regional layer aerodynamic resistance, and then wind speed at a standard reference level (2 m). Blending height is the height above the ground where the influence of local-scale surface heterogeneity upon atmospheric turbulence is relatively unimportant (e.g., Mahrt, 2000). Air temperature is assumed to be a linear function of surface temperature. The slope and offset of this function are derived considering both wet and dry areas. Over the driest areas, LE flux is zero, allowing retrieval of H as a residual of $R_n - G$. Over the wettest areas, H is negligible, with surface temperature equal to near surface air temperature. Key assumptions for SEBAL are the simultaneous presence of wet and dry areas within the remote-sensing scene and the ability to parameterize land-surface resistance with a factor called kB^{-1} (Garratt and Hicks, 1973). This factor is a means for obtaining thermal heat roughness from momentum roughness. Further details of SEBAL can be found in Bastiaanssen et al. (1998a), Su et al. (1999),and Jacob et al. (2002a).

4 Intercomparison Results at SMACEX 2002

Results from the ASTER-based model intercomparison between TSEB and SEBAL model estimates are summarized as cross-plot comparisons on a pixel-by-pixel basis (Fig. 6). These plots help identify how model estimates relate

to each other by flux component and represent frequency counts of the components R_n (upper left), G (upper right), H (lower left) and LE (lower right). The plotted distributions represent spatially comparative SEBAL vs. TSEB fluxes for corn and soybean fields over an area approximately 13 km x 8 km over the Walnut Creek watershed. This subset corresponds to ∼13,000 ASTER pixels. The pixel frequency counts in Fig. 6 were binned according to range of observed fluxes with highest occurrence frequencies coded dark gray.

In aggregate, R_n estimates by SEBAL and TSEB show moderate systematic agreement ($R^2 = 0.68$), but show a bias of 13 W m^{-2}. For soil heat flux G, TSEB and SEBAL calculations are strongly correlated ($R^2 = 0.95$), moderate bias of 11 W m^{-2}, but have differing sensitivities. Where G values are less than ∼100 W m^{-2}, SEBAL and TSEB values agree within standard error of mean values of 8 W m^{-2}, but with G greater than 100 W m^{-2}, SEBAL estimates are on the order of 50 W m^{-2} greater than TSEB estimates. The relationships between turbulent fluxes H and LE are similarly systematic, but with greater differences between low flux values and high flux values. For H estimates, the two models showed good correlation ($R^2 = 0.80$), and bias of 33 W m^{-2}. However, SEBAL model sensitivity was greater than that of TSEB, where the crossplot slope is 1.46, yielding flux estimates differing by over 100 W m^{-2}. The LE comparison results complement the H results, also with good correlation ($R^2 = 0.89$), overall bias of 8 W m^{-2}, and greater SEBAL model sensitivity (crossplot slope of 1.25).

5 Model Validation Results

To evaluate model flux estimates independently of each other, comparisons with ground measured fluxes are needed. Using remote-sensing derived model fluxes and footprint-weighted ground based E-C measurements, flux components are compared for 8 ground locations within the SMACEX experimental area (Table 1, see locations in Fig. 2). The table is divided into four groups, one for each flux component (H, LE, G and R_n). Within each group are 1/2 hourly averaged ground flux values (O) and TSEB (T) and SEBAL (S) flux values. The leftmost column contains the ground station identifier, appended by crop cover (C=corn, S=soybean). The bottom row contains mean flux estimate deviations from E-C measurements when considering all 8 stations. Ground observations for R_n are from tower-mounted net radiometers. G values are from soil heat flux plates. Preliminary turbulent fluxes, H and LE, are from E-C flux observations, nominally 2 m above the ground in soybean fields, and 4 m above the ground in corn fields (Kustas et al., 2004). In rough terms, E-C measurements are represented by no more than ∼4 ASTER pixels in the upwind direction. Energy budgets at all stations were closed by the Bowen ratio approach (Twine et al., 2000), then adjusted for wind speed, wind direction and fetch effects using a flux footprint model from Schuepp et al. (1990).

Comparisons of E-C footprint weighted turbulent fluxes show both models sometimes produce very good agreement over both corn and soybean land-cover types, indicating that integration of ASTER data with an energy flux model is producing useful output. The range of observed conditions spanned cover conditions from sparse (e.g., site 161, soybeans) to thick (e.g., site 151,

corn), with H values ranging between 209 to 47 W m^{-2}. Corresponding LE values ranged between 253 and 463 W m^{-2}. For this example, TSEB results showed better agreement with ground observations of H relative to SEBAL results, where average TSEB deviations were small, 7 W m^{-2}, while SEBAL H deviations were moderate, 89 W m^{-2}. When considering LE estimates, SEBAL returned better results, with an average deviation of 1 W m^{-2}, in comparison with TSEB's average deviation of 89 W m^{-2}.

6 Discussion

In light of the excellent retrieval capabilities of ASTER and the reasonably good agreement between modeled estimates over the SMACEX study site we can say that ASTER is performing consistently. ASTER data provide one of the few avenues to evaluate and test remote sensing-based surface energy flux models at higher resolutions. Spatially varying surface temperatures closely correspond to observed variations in vegetation densities and surface fluxes. Spatial resolution of ASTER resolves physically distinct land-cover types that in the Iowa study have a dominant length scale of 250 m. Without the 15- to 90-m resolution capabilities, flux modeling would have necessitated more empiricism, and therefore more calibration than currently used in the TSEB and SEBAL models. Furthermore, without the higher-resolution images, model comparisons against ground observation sites would not be very meaningful.

Energy flux model intercomparison shows functional relationships exist between the SEBAL and TSEB, indicating both are responding similarly to ASTER temperature, NDVI and albedo input data. However, in general terms, SEBAL predicted fluxes are more sensitive to input changes than are TSEB

predicted fluxes. For example, over low H regions, SEBAL and TSEB commonly agree within 20 W m^{-2}, but over high H regions, SEBAL predicts values up to 200 W m^{-2} greater than TSEB values. Spatial representation of this sensitivity difference is also strongly expressed with LE estimates (Fig. 5). Distributional patterns are similar for both models, but in the SEBAL case, estimated LE areal values are much less than TSEB estimates.

General results from the tabular data shows cross-comparison results seen previously. Agreement between R_n ground observations, and model estimates from TSEB and SEBAL are acceptable with mean deviations of 31 W m^{-2} or less, indicating realistic model estimation of both short- and long-wave radiation components. We note, however, that poor agreement would have been surprising because modeled estimates had the benefit of calibrated spatial albedo data and measured incoming solar radiation. Agreement between G observations and modeled estimates was also good, with average deviation of 15 W m^{-2}. This good agreement indicates that fractional estimation of net radiation based upon NDVI-derived fractional cover works well for the SMACEX area at satellite overpass time.

Agreement for turbulent fluxes H and LE was more problematic to assess. In some cases, (e.g., dense corn field sites 6 and 151), SEBAL LE model results agreed very closely with ground observations ($<$ 10 W m^{-2}), while TSEB results showed differences on the order of 50 W m^{-2}. But in other cases (e.g., sparse soybean field sites 3 and 23), TSEB model results were in much better agreement with E-C observations. TSEB differences for H estimates were typically within 35 W m^{-2} of E-C values, while SEBAL estimates were highly discrepant (up to 150 W m^{-2}).

Because these flux estimate discrepancies arise from identical input data, their causes have to be explained by TSEB/SEBAL model differences and assumptions. One important model difference lies with model representation of land and near surface air temperatures. In TSEB, H was determined by the gradient between observed land surface radiometric temperatures and an observed air temperature. At SMACEX a constant near surface air temperature was used with TSEB, meaning that modeled H values were directly related to observed radiometric surface temperatures. Based on the 7 W m^{-2} average deviation between E-C and TSEB H fluxes, this gradient estimation approach seems accurate within E-C measurement error. By contrast, the SEBAL model, returned comparatively less accurate H estimates, with an average deviation of 89 W m^{-2}. SEBAL does not use near surface air temperatures because of its temperature normalization using wet and dry areas. Though known to work well elsewhere, the application of this approach did not work well at SMACEX due to an inability to fully distinguish wet and dry areas. As noted previously, SEBAL anticipates a parabolic relationship between surface temperature and albedo, thus distinguishing evaporative and radiative controlled domains. At SMACEX this parabolic relationship did not exist (Fig. 7), despite known existence of sparsely vegetated and riparian zones. This means successful retrieval by SEBAL of meteorological and resistance parameters is questionable because no distinction between minimum and maximum temperatures within the radiative and evaporative domains is possible for this 1 July scene.

Current validation results at SMACEX suggest more accurate flux estimation from TSEB than from SEBAL (Table 1). As noted, typical H estimates from TSEB were within 7 W m^{-2} of ground observations, while typical LE estimates from TSEB deviated significantly less from observations than did SEBAL

estimates. Most of the disagreements between TSEB and SEBAL estimates occurred over sparsely vegetated sites, suggesting that the soil-vegetation differentiation accommodated by TSEB is a significant model benefit.

Nevertheless, some caution is required with these results. especially considering the preliminary nature of surface flux observations. Issues such as energy budget closure and flux footprint estimates need more thorough investigation. Such investigation is underway, which will also consider flux estimates from the SEBS and the NDVI/Temperature triangle approaches.

7 Conclusions

Estimation of spatially distributed surface energy fluxes over agricultural areas requires high-quality remote sensing, a need mostly fulfilled by ASTER. With spatial resolution capabilities ranging between 15 and 90 m, ASTER can detect and discriminate variations in surface temperature, emissivity, vegetation densities and albedo corresponding to distinct land use types and thus reduce problems from mixed-pixels.

In this study we have combined consistent ASTER observations with physically based surface energy flux models to retrieve reasonable estimates of instantaneous surface energy fluxes. Using model intercomparison results showed systematic agreement between all flux components, indicating that the two models tested, TSEB and SEBAL, operate similarly when provided identical remote-sensing inputs. These first results from the multi-model intercomparison study also showed significantly different model sensitivities, indicating a need for further, in-depth analysis of each of model. Such investigations

are possible because of multispectral, high spatial resolution over VNIR-TIR bands observed by ASTER.

8 Acknowledgments

This work would not have been possible without support from the U.S. Water Conservation Lab, NASA EOS Grant 03-OES-02, and the Department of Research, Development, and International Relations of the Purpan Graduate School of Agriculture. We especially thank John Eaton for Octave (www.octave.org) and the many contributors to the R project (www.r-project.org) for providing superb open-source software.

References

Abrams, M., 2000. The Advanced Spaceborne Thermal Emission and Reflection radiometer (ASTER): Data products for the high spatial resolution imager on NASA's Terra platform. International Journal of Remote Sensing 21, 847–859.

Anderson, M., Norman, J., Diak, G., Kustas, W., Mecikalski, J., 1997. A two-source time-integrated model for estimating surface fluxes from thermal infrared satellite observations. Remote Sens. Environ. 60, 195–216.

Bastiaanssen, W., Menenti, M., Feddes, R., Holtslag, A., 1998a. A remote sensing surface energy balance algorithm for land (SEBAL) 1. Formulation. Journal of Hydrology 212-213, 198–212.

Bastiaanssen, W., Pelgrum, H., Wang, J., Ma, Y., Moreno, J., Roerink, G.,

van der Wal, T., 1998b. A remote sensing surface energy balance algorithm for land (SEBAL). II: Validation. Journal of Hydrology 212-213, 213–292.

Berk, A., Bernstein, L., Anderson, G., Acharya, P., Robertson, D., Chetwynd, J., Adler-Golden, S., 1998. MODTRAN cloud and multiple scattering upgrade with application to AVIRIS. Remote Sens. Environ. 65, 367–375.

Brutsaert, W., 1982. Evaporation into the atmosphere: theory, history and applications. D. Reidel Pub. Co., Dordrecht, Holland.

French, A. N., Schmugge, T. J., Kustas, W. P., Brubaker, K. L., Prueger, J., 2003. Surface energy fluxes over El Reno, Oklahoma, using high-resolution remotely sensed data. Water Resour. Res. 39 (6), 1164.

Garratt, J., Hicks, B., 1973. Momentum, heat and water vapour transfer to and from natural and artificial surfaces. Q.J.R. Meteorol. Soc. 99, 680–687.

Gillespie, A., Rokugawa, S., Matsunaga, T., Cothern, J., Hook, S., Kahle, A., 1998. A temperature and emissivity separation algorithm for advanced spaceborne thermal emission and reflection radiometer (ASTER) images. IEEE Trans. Geosci. Remote Sens. 36, 1113–1126.

Gillies, R., Carlson, T., Cui, J., Kustas, W., Humes, K., 1997. A verification of the triangle method for obstaining surface soil water content and energy fluxes from remote measurements of the Normalized Difference Vegetation Index NDVI and surface radiant temperature. Int. J. Remote Sensing 18 (15), 3145–3166.

Goudriaan, J., 1977. Crop micrometeorology: a simulation study. Tech. rep., Centre for Agricultural Publishing and Documentation, Wageningen.

Goutorbe, J.-P., Lebel, T., Tinga, A., Bessemoulin, P., Brouwer, J., Dolman, A., Engman, E., Gash, J., Hoepffner, M., Kabat, P., Kerr, Y., Monteney, B., Prince, S., Said, F., Sellers, P., Wallace, J., 1994. HAPEX-Sahel: a large scale study of land-atmosphere interactions in the semi-arid tropics. Ann.

Geophys. 12, 53–64.

Hall, F., Huemmrich, K., Goetz, S., Sellers, P., Nickerson, J., 1992. Satellite remote sensing of surface energy balance: sucess, failures and unresolved issues in FIFE. J. Geophys. Res. 97, 19061–19089.

Halldin, S., Gryning, S.-E., December 1999. Boreal forests and climate. Agric. For. Meteorol. 98-99, 1–4.

Hasager, C., Jensen, N. O., Olioso, A., 2002. Land cover, surface temperature and leaf area index maps from satellites used for the aggregation of momentum and temperature roughnesses. In: Sobrino, J. (Ed.), Proceedings of the First International Symposium on Recent Advances in Quantitative Remote Sensing, September 2002, Valencia, Spain. pp. 466–473.

Havstad, K., Kustas, W., Rango, A., Ritchie, J., Schmugge, T., 2000. Jornada experimental range: a unique arid land location for experiments to validate satellite systems. Remote Sens. Environ. 74 (1), 13–25.

Hook, S., Prata, F., 2001. Land surface temperature measured by ASTER-first results. In: Geophysical Research Abstracts, 26th General Assembly. Vol. 3. European Geophysical Society, p. 71.

Jackson, R., Reginato, R., Idso, S., 1977. Wheat canopy temperature: a practical tool for evaluating water requirements. Water Resour. Res. 13, 651–656.

Jacob, F., Olioso, A., Gu, X., Su, Z., Seguin, B., 2002a. Mapping surface fluxes using airborne visible, near infrared, thermal infrared remote sensing and a spatialized surface energy balance model. Agronomie 22, 669–680.

Jacob, F., Petitcolin, F., Schmugge, T., Vermote, E., Ogawa, K., French, A., 2004. Comparison of land surface emissivity and radiometric temperature from MODIS and ASTER sensors. Remote Sensing of Environment 83, 1–18.

Jacob, F., Schmugge, T., Ogawa, K., A., F., Ritchie, J., 2002b. The poten-

tialities of ASTER to retrieve radiative properties over semi-arid regions. In: Sobrino, J. (Ed.), First International Symposium on Recent Advances in Quantitative Remote Sensing. pp. 913–920.

Kanemasu, E., Verma, S., Smith, E., adn M. Wesely, L. F., Field, R., Kustas, W., Weaver, H., Steward, J., Gurney, R., Panin, G., Moncrieff, J., 1992. Surface fluxes measurements in FIFE: an overview. J. Geophys. Res. 97(D17), 18547–18555.

Kustas, W., Humes, K., Norman, J., Moran, M., 1996. Single and dual source modeling of surface energy fluxes with radiometric surface temperature. Journal of Applied Meteorology 35, 110–121.

Kustas, W., Li, F., Jackson, T., Prueger, J., MacPherson, J., Wolde, M., 2004. Effects of remote sensing pixel resolution on modeled energy flux variability of croplands in Iowa. Remote Sens. Environ. 92, 535–547.

Kustas, W., Norman, J., 1996. Use of remote sensing for evapotranspiration monitoring over land surfaces. Hydrological Sciences 41 (4), 495–516.

Kustas, W., Perry, E., Doraiswamy, P., Moran, M., 1994. Using satellite remote sensing to extrapolate evapotranspiration estimates in time and space over a semiarid rangeland basin. Remote Sens. Environ. 49, 275–286.

Kustas, W. P., Norman, J. M., 1999. Reply to comments about the basic equations of dual-source vegetation-atmosphere transfer models. Agric. For. Meteorol. 94, 275–278.

Kustas, W. P., Norman, J. M., 2000. A two-source energy balance approach using directional radiometric temperature observations for sparse canopy covered surfaces. Agronomy Journal 92 (5), 847–854.

Kustas, W. P., Norman, J. N., Anderson, M. C., French, A. N., 2003. Estimating subpixel surface temperatures and energy fluxes from the vegetation index-radiometric temperature relationship. Remote Sens. Environ. 85, 429–

440.

Mahrt, L., 2000. Surface heterogeneity and vertical structure of the boundary layer. Boundary-Layer Meteorol. 96, 33–62.

McNaughton, K., Spriggs, T., 1989. An evaluation of the Priestley-Taylor equation and the complementary relationship using results from a mixed-layer model of the convective boundary layer. In: Black, T., Spittlehouse, D., Novak, M., Price, D. (Eds.), Estimation of areal evapotransiration. No. 177. Internation Association of Hydrological Sciences, pp. 89–103, proceedings of a workshop held at Vancouver, B.C., Canada, August 1987.

Mecikalski, J., Diak, G., Anderson, M., Norman, J., September 1999. Estimating fluxes on continental scales using remotely sensed data in an atmospheric-land exchange model. J. Appl. Met. 38 (9), 1352–1369.

Meyers, T., Hollinger, S., 2004. An assessment of storage terms in the surface energy balance of maize and soybean. Agric. For. Meteorol. in press.

Monteith, J., Unsworth, M., 1990. Principles of Environmental Physics, 2nd Edition. Edward Arnold.

Moran, M., Kustas, W., Vidal, A., Stannard, D., Blanford, J., Nichols, W., 1994. Use of ground-based remotely sensed data for surface energy balance evaluation of a semiarid rangeland. Water Resources Research 30, 1339–1349.

Norman, J., Anderson, M., Kustas, W., French, A., Mecicalski, J., Torn, R., Diak, G., Schmugge, T., Tanner, B., 2003. Remote sensing of surface energy fluxes at 10^1-m pixel resolutions. Water Resour. Res. 39, 1221.

Norman, J., Kustas, W., Humes, K., 1995. A two-source approach for estimating soil and vegetation energy fluxes from observations of directional radiometric surface temperature. Agric. For. Meteorol. 77, 263–293.

Norman, J., Kustas, W., Prueger, J., Diak, G., August 2000. Surface flux

estimation using radiometric temperature: A dual- temperature-difference method to minimize measurement errors. Water Resour. Res. 36 (8), 2263–2274.

Olioso, A., Braud, I., Chanzy, A., Courault, D., Demarty, J., Kergoat, L., Lewan, L., Ottl, C., Prvot, L., Zhao, W., Calvet, J., Cayrol, P., Jongschaap, R., Moulin, S., Noilhan, J., Wigneron, J.-P., 2002a. SVAT modeling over the Alpilles-ReSeDA experiment: comparison of SVAT models over wheat fields. Agronomie: Agriculture and Environment 22, 651–668.

Olioso, A., Braud, I., Chanzy, A., Demarty, J., Ducros, Y., Gaudu, J., Gonzales-Soza, E., Lewan, L., Marloie, O., Ottl, C., Prvot, L., Thony, J.-L., Autret, H., Bethenod, O., Bonnefond, J.-M., Brugier, N., Buis, J.-P., Calvet, J.-C., Caselles, V., Chauki, H., Coll, C., Francois, C., Goujet, R., Jongschaap, R., Kerr, Y., King, C., Lagouarde, J.-P., Laurent, J., Lecharpentier, P., McAnneney, J., Moulin, S., Rubio, E., Weiss, M., Wigneron, J.-P., 2002b. Monitoring energy and mass transfers during the Alpilles-ReSeDA experiment. Agronomie: Agriculture and Environment 22, 597–610.

Pelgrum, H., Bastiaanssen, W., 1996. An inter-comparison of techniques to determine the area-averaged latent heat flux from individual in situ observations : a remote sensing approach using the European Field Experiment in a Desertification-threatened Area data. Water Resources Research 32, 2775–2786.

Penman, H., 1948. Natural evaporation from open water, bare soil and grass. Proc. R. Soc. London 193, 120–145, series A.

Priestley, C., Taylor, R., 1972. On the assessment of surface heat flux and evaporation using large-scale parameters. Monthly Weath. Rev. 100, 81–92.

Schuepp, P., Leclerc, M., MacPherson, J., Desjardins, R., 1990. Footprint prediction of scalar fluxes from analytical solutions of the diffusion equation.

Boundary-Layer Meteorol. 50, 355–373.

Seguin, B., Becker, F., Phulpin, T., Gu, X., Guyot, G., Kerr, Y., King, C., Lagouarde, J., Ottlé, C., Stoll, M., Tabbagh, T., Vidal, A., 1999. IRSUTE: A minisatellite project for land surface heat flux estimation from field to regional scale. Remote Sens. Environ. 68, 357–369.

Sellers, P., Hall, F., Kelly, R., Black, A., Baldocchi, D., Berry, J., Ryan, M., Ranson, K., Crill, P., Lettenmaier, D., Margolis, H., Cihlar, J., Newcomer, J., Fitzjarrald, D., Jarvis, P., Gower, S., Halliwell, D., Williams, D., Goodison, B., Wickland, D., Guertin, F., 1997. BOREAS in 1997: Experiment overview, scientific results and future directions. J. Geophys. Res. 102 (D24), 28731–28770.

Sellers, P., Mintz, Y., Sud, Y., Dalcher, A., 1986. A simple biosphere model (SiB) for use within general circulation models. J. Atmos. Sci. 43, 505–531.

Shuttleworth, W., Gurney, R., Hsu, R., Ormsby, J., 1989. FIFE : the variation in energy partitioning at surface flux sites. In: Remote sensing and large scale global processes proceedings, Baltimore symposium, IAHS publications. pp. 67–74.

Stannard, D., Blanford, J., Kustas, W., Nichols, W., Amer, S., Schmugge, T., Wetlz, M., 1994. Interpretation of surface fluxes measurements in heterogeneous terrain during the Monsoon '90 experiment. Water Resources Research 30, 1227–1239.

Su, S., Pelgrum, H., Menenti, M., 1999. Aggregation effects of surface heterogeneity in land surface processes. Hydrology and Earth System Sciences 3 (4), 549–563.

Su, Z., 2002. The surface energy balance system (SEBS) for estimation of the turbulent heat fluxes. Hydrology and Earth Sciences 6 (1), 85–99.

Twine, T., Kustas, W., Norman, J., Cook, D., Houser, P., Meyers, T., Prueger,

J., Starks, P., Wesely, M., 2000. Correcting eddy-covariance flux underestimates over a grassland. Agric. For. Meteorol. 103, 279–300.

Wassenaar, T., Olioso, A., Hasager, C., Jacob, F., Chehbouni, A., 2002. Estimation of evapotranspiration over heterogeneous pixels. In: Sobrino, J. (Ed.), Proceedings of the First International Symposium on Recent Advances in Quantitative Remote Sensing, September 2002, Valencia, Spain. pp. 458–465.

Woodcock, C. E., Strahler, A. H., 1987. The factor of scale in remote sensing. Remote Sens. Environ. 21, 311–332.

Yamaguchi, Y., Kahle, A., Tsu, H., Kawakami, T., Pniel, M., 1998. Overview of Advanced Space-borne Thermal Emission and Reflection Radiometer (ASTER). IEEE Transactions on Geoscience and Remote Sensing 36, 1282–1289.

Zhan, X., Kustas, W., Humes, K., 1996. An intercomparison study on models of sensible heat flux over partial canopy surfaces with remotely sensed surface temperature. Remote Sens. Environ. 58, 242–256.

List of Figures

1 ASTER NDVI over SMACEX site on 1 July 2002. NDVI values range from 0.3 (white) to 0.9 (black), respectively sparse vegetation and thick vegetation. E-C tower locations are indicated by white circles. Nested squares at upper right indicate sizes of 250-m and 1-km pixels. This scene and subsequent ones are projected to UTM zone 15 coordinates. The white area at the left denotes the edge of the ASTER scene. 33

2 ASTER surface temperature over SMACEX site on 1 July 2002. Temperatures range from 25°C (dark gray) to 40°C (white). Numbered points indicate field campaign E-C station locations. 34

3 NDVI histograms of SMACEX at 15-, 90- and 240-m resolutions. Bi-modal distributions for 15-m and 90-m images reflect the known land cover patterns of relatively sparse soybean fields and dense corn fields. The distribution becomes uni-modal at 240-m resolution, meaning that most pixels are mixed at this coarser observational scale. 35

4 Spectral properties within longer wavelengths of the TIR window. Lines represent, from top to bottom: example dry silt-loam soil emissivity (Emis.), from central Oklahoma, example atmospheric transmissivity (Trans.), from a SMACEX radiosonde, filter response (Resp.) functions for ASTER bands 13 and 14 (solid) and TM7 band 6 (dashed). Response functions have been scaled by $\frac{1}{3}$ to aid display. 36

5 Latent heat fluxes (LE) from SEBAL (left) and TSEB (right) models over the 1 July 2002 Iowa SMACEX study area. Both models show LE patterns consistent with patterns seen in Figs. 1 and 2, but average ET flux estimates from SEBAL are commonly $\frac{1}{2}$ to $\frac{1}{3}$ of TSEB estimates. Displays are scaled from 0 (black) to 600 W m^{-2} (white). 36

6 Joint distribution of SEBAL and TSEB modeled fluxes over SMACEX by component. Shown are R_n, net radiation (upper left), G, soil heat flux (upper right), H, sensible heat flux (lower left), and LE, latent heat flux (lower right) in W m^{-2}. Darker grays represent highest occurrence frequencies. 37

7 Temperature vs. albedo distribution plot over SMACEX, 1 July 2002 showing mostly constant albedo values for temperatures between 30 and 40°C . This distribution falls within the radiative controlled domain. 38

Table 1

Eddy Covariance (E-C) measurements vs. TSEB & SEBAL model estimates over 8 SMACEX sites. E-C measurements are half-hourly averages taken around ASTER overpass time, 15:12 UTC, 1 July 2002. Model estimates are footprint weighted, considering wind speed and wind direction at the E-C measurement height. E-C site identifiers (Stn) and crop type (C: corn, S: soybean) are in the left-most column, followed by column groups for each flux component: sensible heat, H; latent heat, LE; soil heal, G; and net radiation, R_n. Within each flux type are listed E-C measurements (O), TSEB estimates (T), and SEBAL estimates (S). The final tabulated row ($\overline{\Delta}$) shows average deviations between E-C values and modeled estimates.

Stn	H			LE			G			R_n		
	O	T	S	O	T	S	O	T	S	O	T	S
3S	150	179	318	277	323	206	105	112	82	637	615	606
6C	79	70	101	479	534	483	63	64	44	660	668	628
151C	77	88	127	463	520	468	66	64	46	657	672	641
152C	96	96	141	363	513	457	47	62	46	652	671	644
161S	209	174	311	253	336	215	92	117	83	642	626	609
23S	125	142	305	299	367	204	63	118	83	660	627	591
24C	47	71	126	401	532	453	47	63	45	642	666	624
33C	97	111	164	371	491	416	63	67	50	667	669	630
$\overline{\Delta}$		7	89		89	-1		15	-8		0	-31

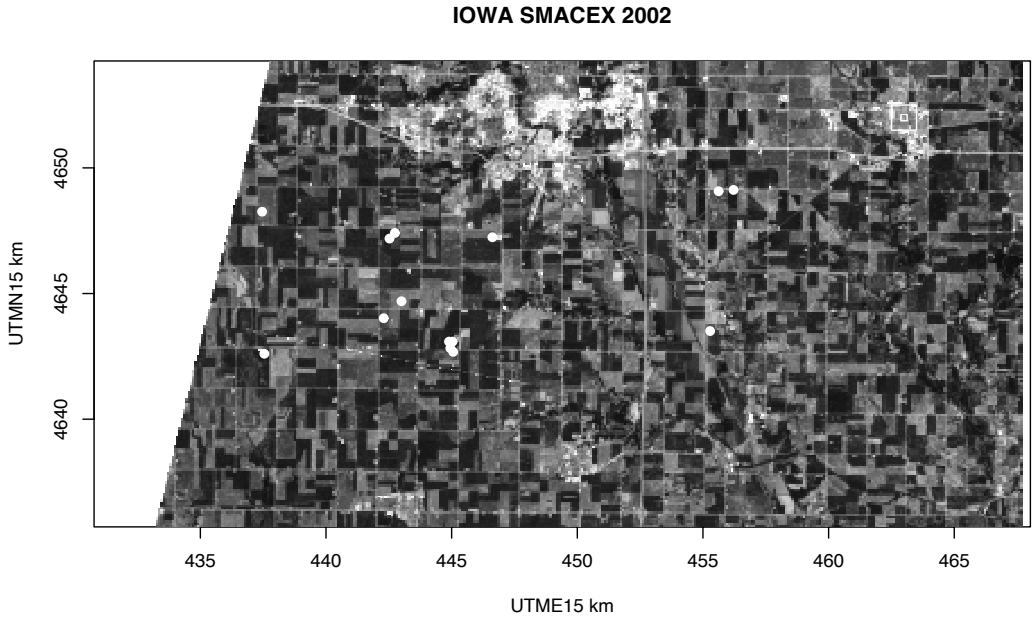

Fig. 1. ASTER NDVI over SMACEX site on 1 July 2002. NDVI values range from 0.3 (white) to 0.9 (black), respectively sparse vegetation and thick vegetation. E-C tower locations are indicated by white circles. Nested squares at upper right indicate sizes of 250-m and 1-km pixels. This scene and subsequent ones are projected to UTM zone 15 coordinates. The white area at the left denotes the edge of the ASTER scene.

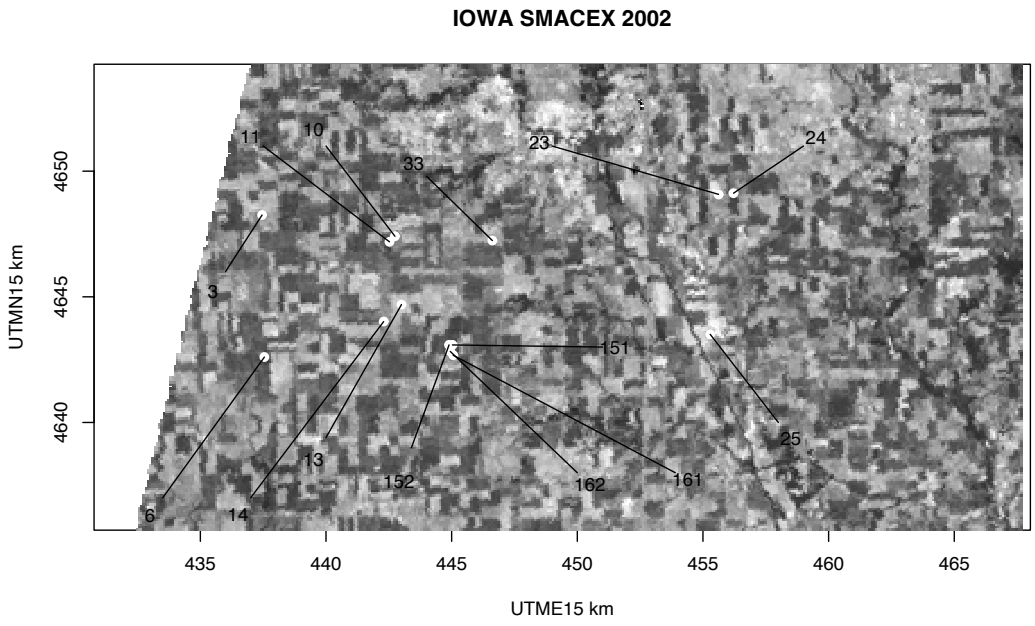

Fig. 2. ASTER surface temperature over SMACEX site on 1 July 2002. Temperatures range from 25°C (dark gray) to 40°C (white). Numbered points indicate field campaign E-C station locations.

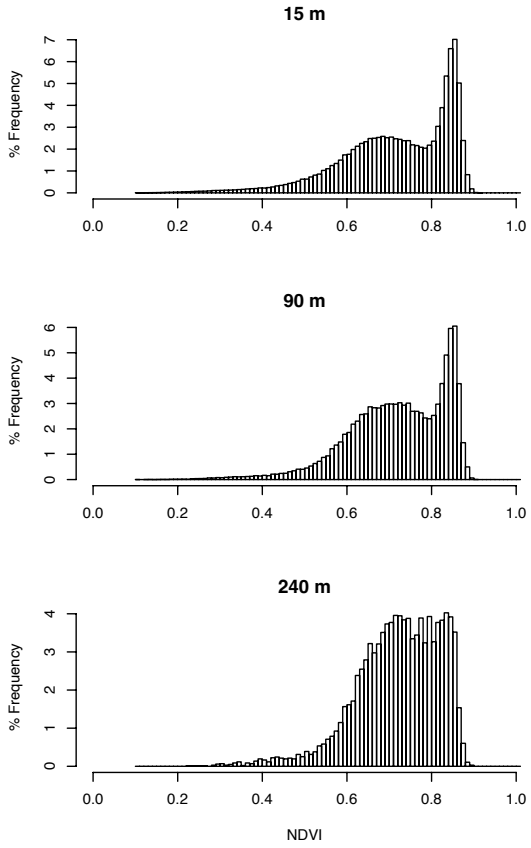

Fig. 3. NDVI histograms of SMACEX at 15-, 90- and 240-m resolutions. Bi-modal distributions for 15-m and 90-m images reflect the known land cover patterns of relatively sparse soybean fields and dense corn fields. The distribution becomes uni-modal at 240-m resolution, meaning that most pixels are mixed at this coarser observational scale.

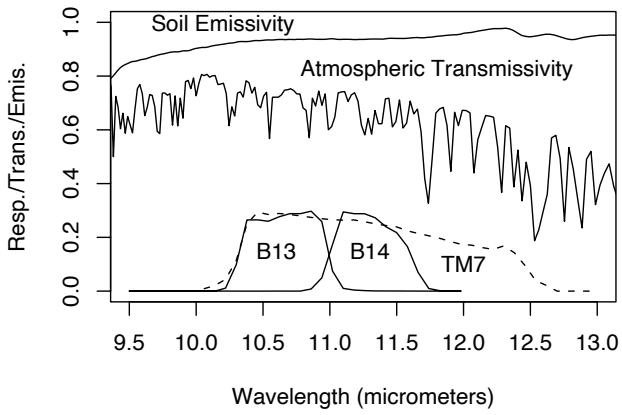

Fig. 4. Spectral properties within longer wavelengths of the TIR window. Lines represent, from top to bottom: example dry silt-loam soil emissivity (Emis.), from central Oklahoma, example atmospheric transmissivity (Trans.), from a SMACEX radiosonde, filter response (Resp.) functions for ASTER bands 13 and 14 (solid) and TM7 band 6 (dashed). Response functions have been scaled by $\frac{1}{3}$ to aid display.

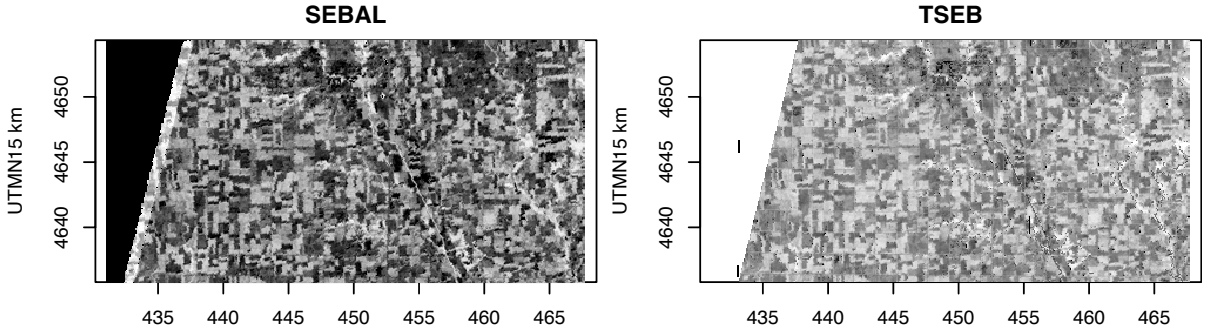

Fig. 5. Latent heat fluxes (LE) from SEBAL (left) and TSEB (right) models over the 1 July 2002 Iowa SMACEX study area. Both models show LE patterns consistent with patterns seen in Figs. 1 and 2, but average ET flux estimates from SEBAL are commonly $\frac{1}{2}$ to $\frac{1}{3}$ of TSEB estimates. Displays are scaled from 0 (black) to 600 W m^{-2} (white).

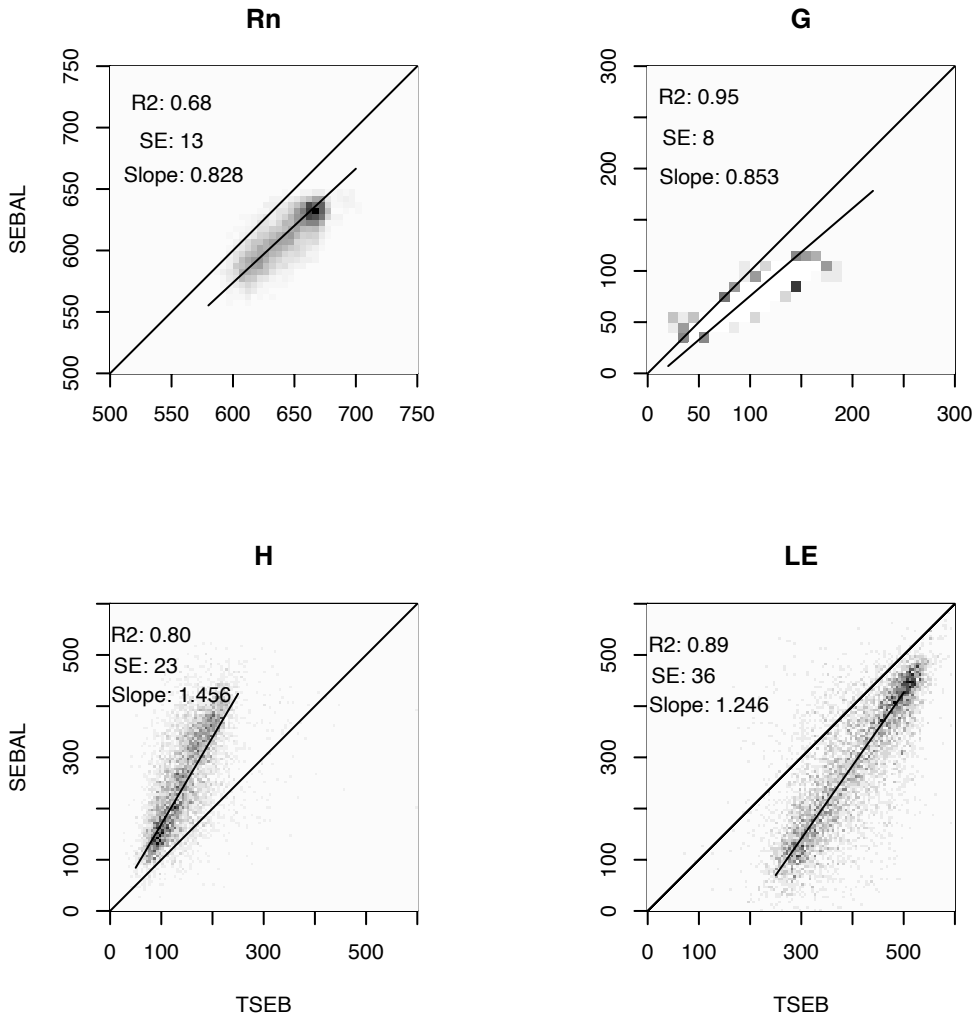

Fig. 6. Joint distribution of SEBAL and TSEB modeled fluxes over SMACEX by component. Shown are R_n, net radiation (upper left), G, soil heat flux (upper right), H, sensible heat flux (lower left), and LE, latent heat flux (lower right) in W m^{-2}. Darker grays represent highest occurrence frequencies.

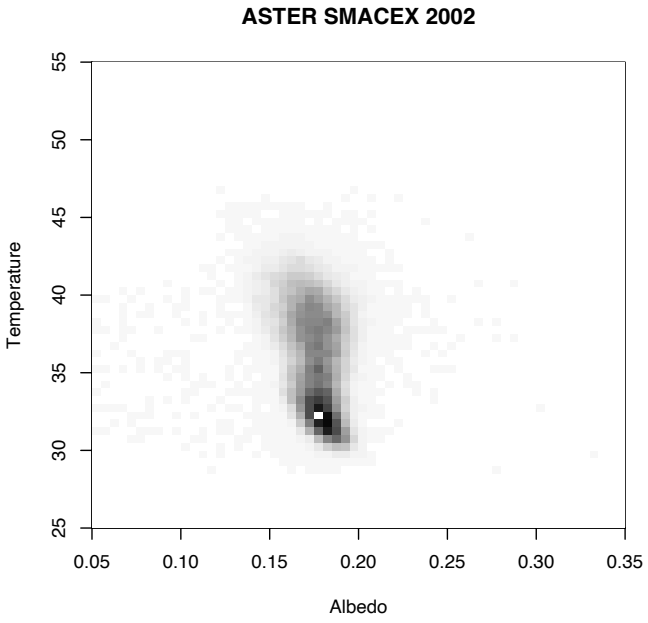

Fig. 7. Temperature vs. albedo distribution plot over SMACEX, 1 July 2002 showing mostly constant albedo values for temperatures between 30 and 40°C . This distribution falls within the radiative controlled domain.

Figures

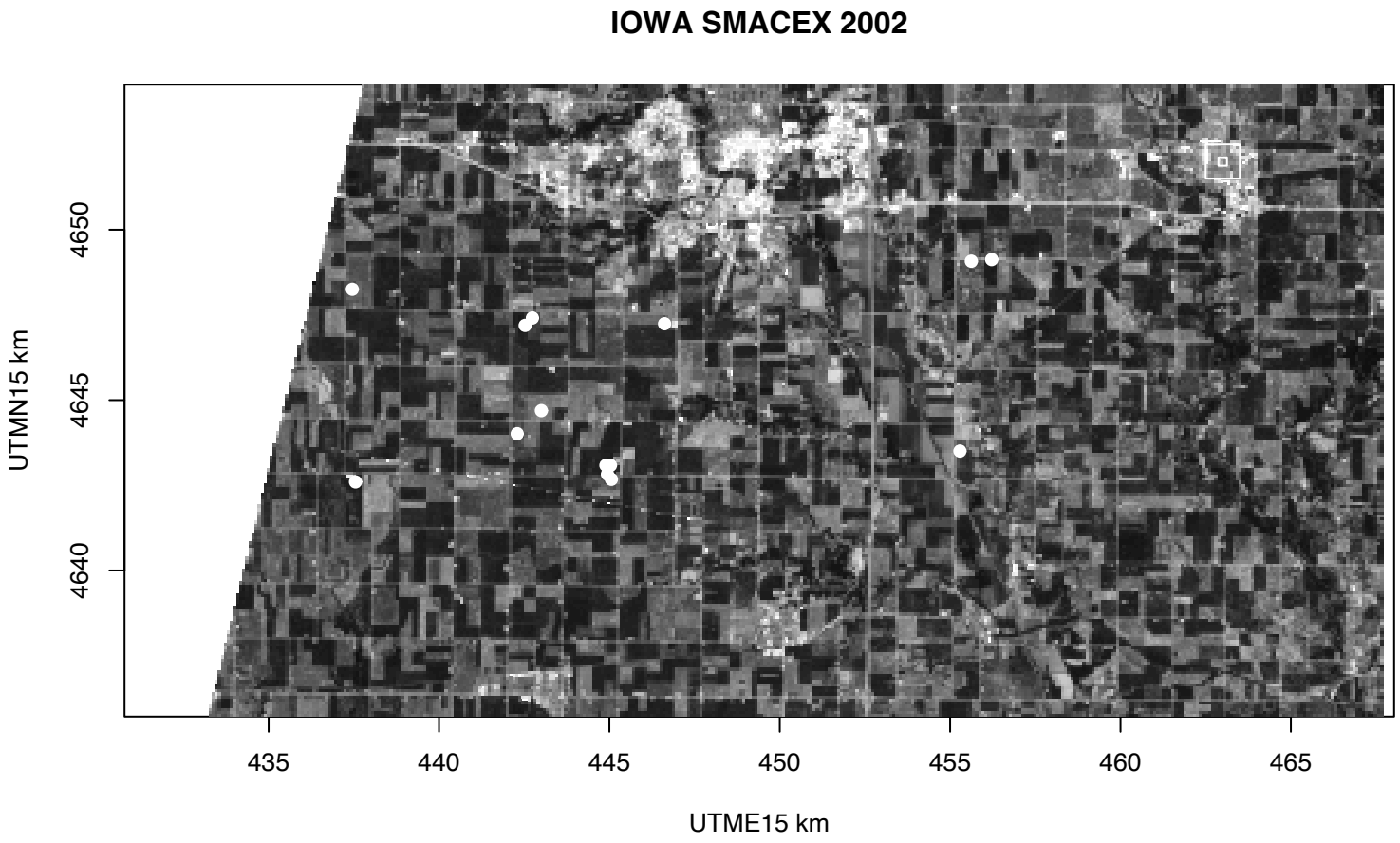
IOWA SMACEX 2002
UTMN15 km
4650
4645
4640
435
440
445
450
455
460
465
UTME15 km

Figures

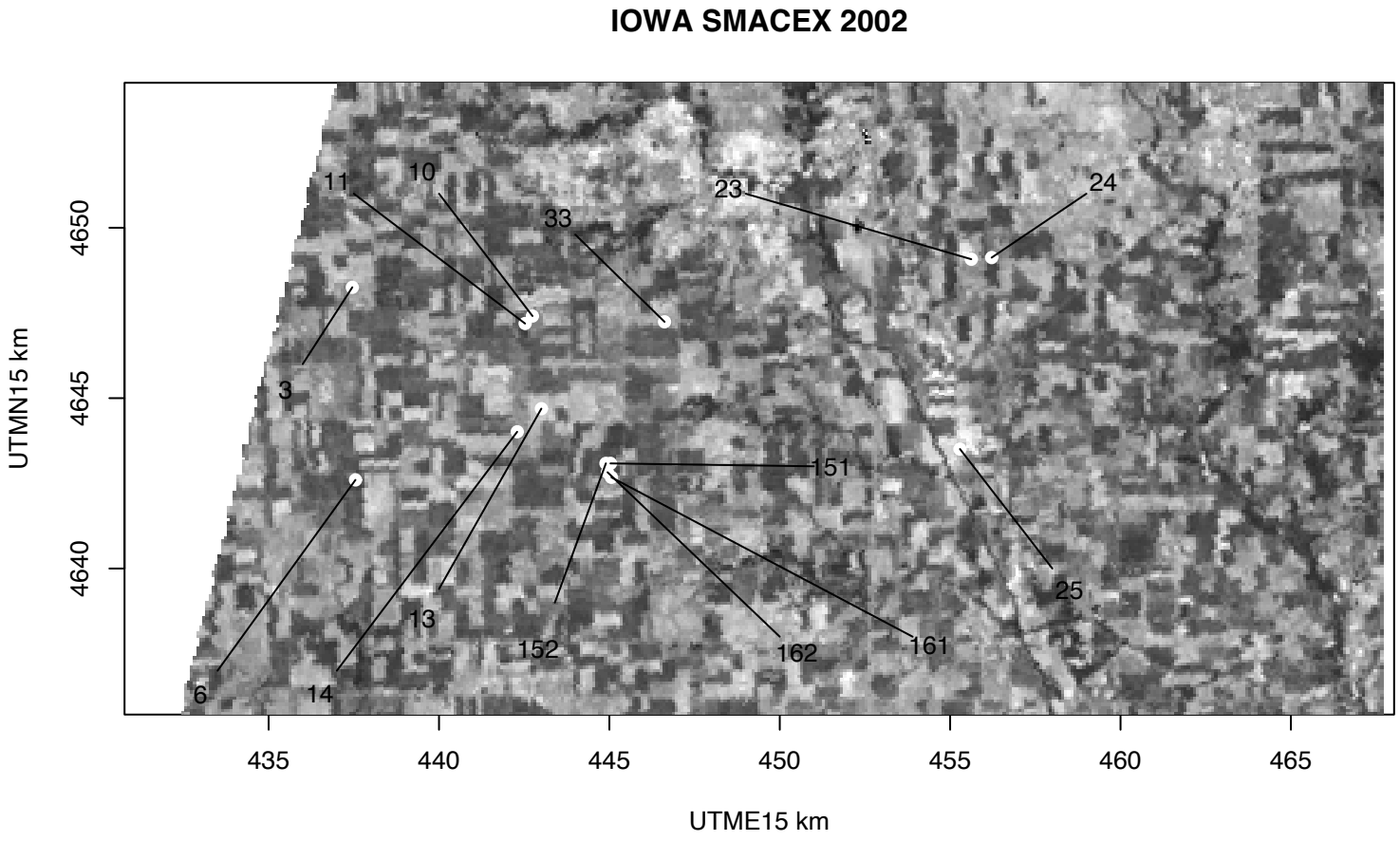
IOWA SMACEX 2002
UTMN15 km
4650
4645
4640
435
440
445
450
455
460
465
UTME15 km
11
10
33
23
24
3
151
25
13
152
162
161
6
14

Figures

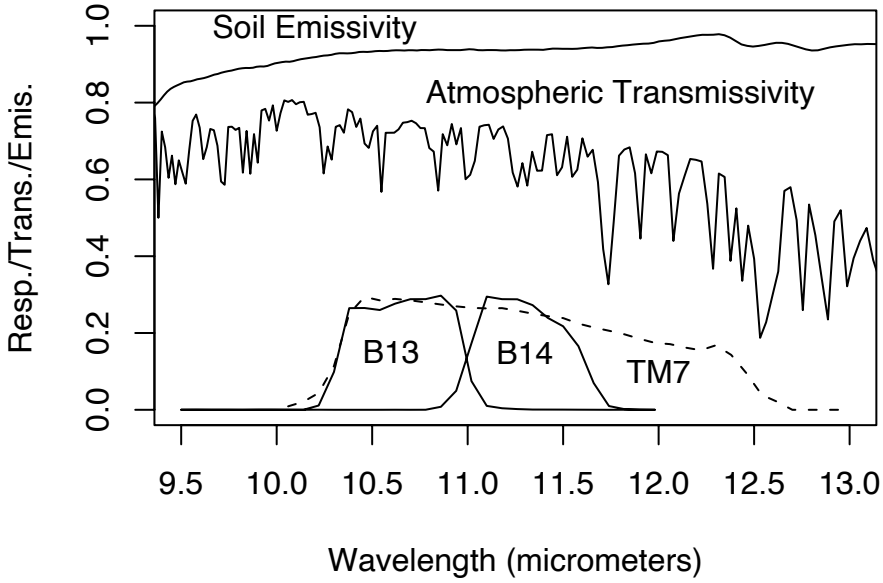
Soil Emissivity
Atmospheric Transmissivity
B13
B14
TM7
Resp./Trans./Emis.
0.0
0.2
0.4
0.6
0.8
1.0
9.5
10.0
10.5
11.0
11.5
12.0
12.5
13.0
Wavelength (micrometers)

Figures

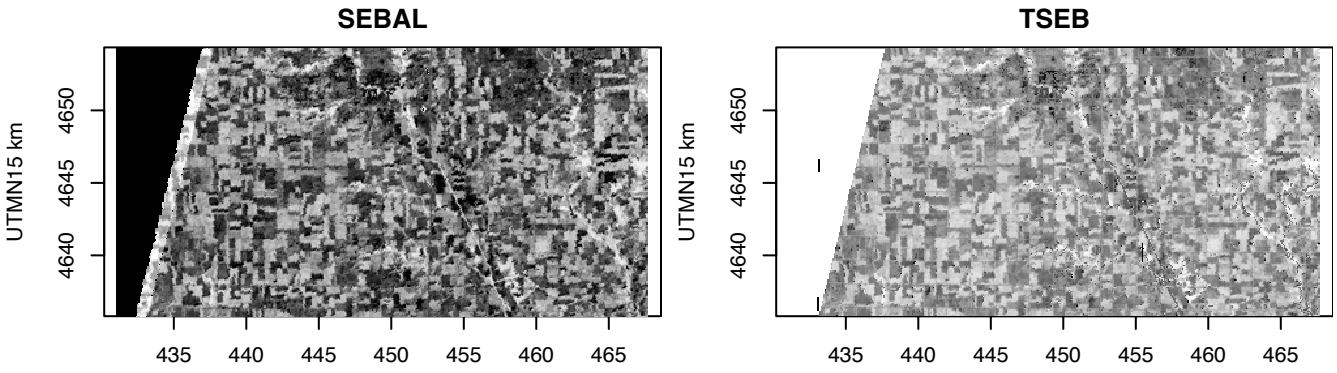
SEBAL
TSEB
UTMN15 km
4640
4645
4650
435
440
445
450
455
460
465

Figures

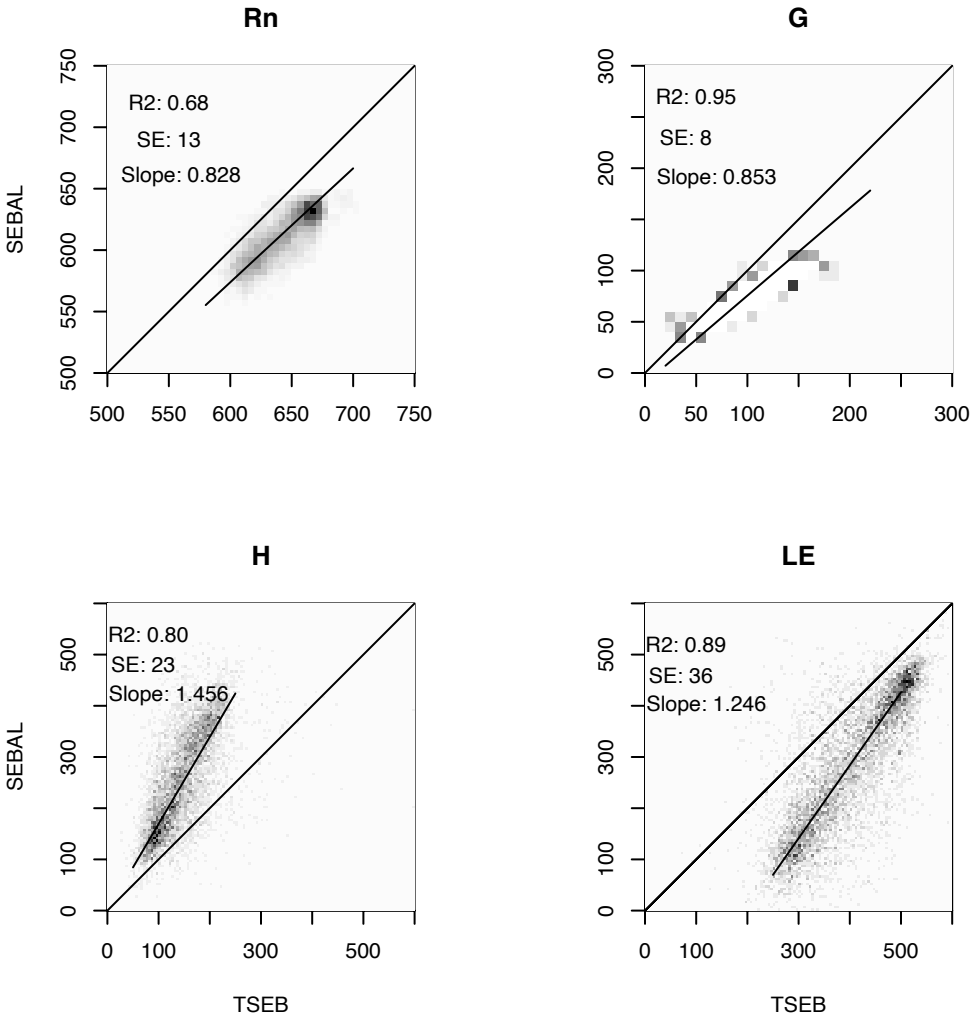
Rn
R2: 0.68
SE: 13
Slope: 0.828
SEBAL
500
550
600
650
700
750
G
R2: 0.95
SE: 8
Slope: 0.853
0
50
100
200
300
H
R2: 0.80
SE: 23
Slope: 1.456
TSEB
LE
R2: 0.89
SE: 36
Slope: 1.246

Figures

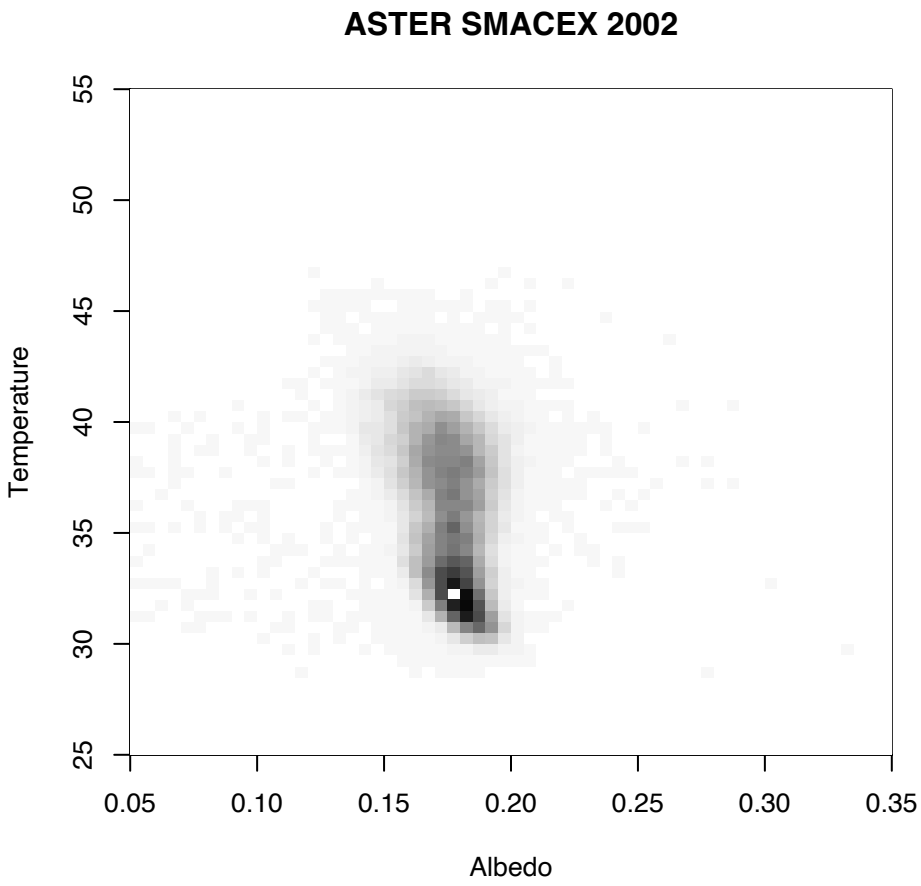
ASTER SMACEX 2002
Temperature
55
50
45
40
35
30
25
0.05
0.10
0.15
0.20
0.25
0.30
0.35
Albedo

Figure 3: NDVI histograms